Light Field Illumination: A Universal Lighting Approach for Visual Inspection

Christian Kludt, Lukas Dippon, Thomas Längle, and Jürgen Beyerer

Fraunhofer IOSB,
Fraunhoferstr. 1, 76131 Karlsruhe

Abstract Choosing a proper lighting approach is a crucial task in designing visual inspection systems. It becomes especially challenging for complex-shaped objects, which change the direction and distribution of incoming light in various ways. We overcome this challenge by constructing a light field display and deploy it as a highly tunable lighting device. By programmatically controlling the spatial position of the individual light sources while simultaneously controlling their angular direction of emission, an object-specific light field can be generated, which highlights the features of the object under test with maximum contrast. We explain the calibration procedure, the rendering pipeline and present first results of the device's performance.

Keywords Light field, visual inspection, programmable lighting, projection calibration, phase-shifting, light field-rendering

1 Introduction

The image processing chain consists of the main components illumination, light-material interaction (transmission, deflection, reflection, scattering, etc.), image acquisition, digitization, data evaluation, classification and finally decision making. For the latter to be carried out robustly, it is crucial to extract the key features of the test object with high contrast. It is usually advantageous to control the image creation process at the beginning, i. e. the illumination. The most common illumination setups are shown in Figure 1.1: bright and dark

field illumination both with front and back lighting. Depending on the direction of the incoming light, different structures of the object are highlighted.

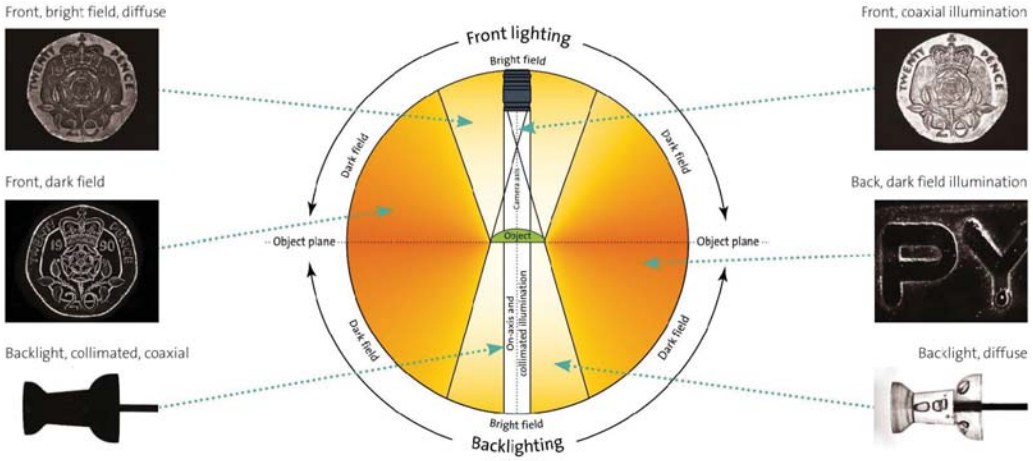

Figure 1.1: Illumination setups. From [1]. By varying the angle of illumination, different structures of the specimen become visible.

However, more complex objects require a more sophisticated illumination setup, which is realized by adding further light sources. Currently, we deploy machine vision systems with more than 64 different lighting channels. Adding, adjusting and testing them is a time consuming process, particularly during system design. Different lighting hardware such as collimated, diffuse, structured and colored lightings have to be evaluated. It would come in handy to have more generic lighting approach in a single device.

2 Existing Approaches

The Purity [2] inspection system at Fraunhofer IOSB utilizes a multichannel imaging system to acquire images from various illumination directions at once. The basic setup is depicted in Figure 2.1. For each kind of defect, a suitable illumination channel is realized which ensures an image with maximum contrast. Opaque inclusion will appear dark in the bright field channel (red), whereas scattering defects such as enclosed air bubbles will appear as bright spots in the dark field image (blue). Scattering defects on the surface, e. g. scratches or dust, become visible under gracing illumination (green).

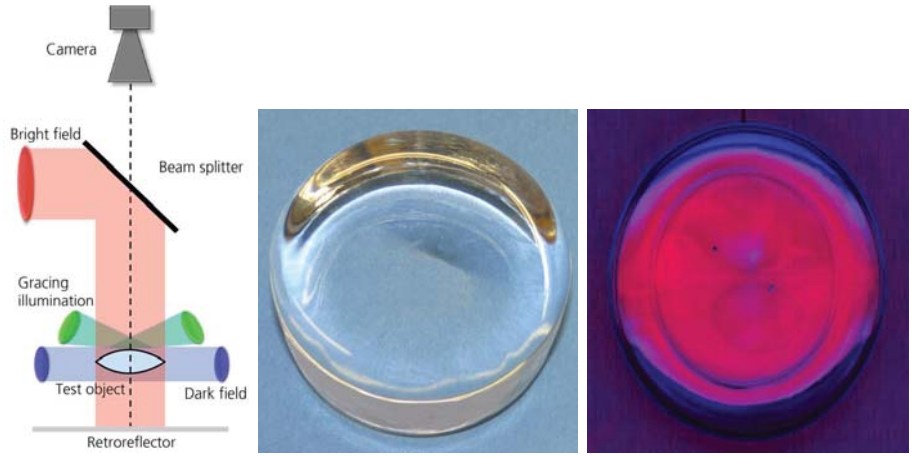

(a) (b) (c)

Figure 2.1: Purity inspection system. From [3]. (a) Basic setup. (b) Transparent test object. (c) Acquisition of different illumination directions simultaneously by means of color multiplexing.

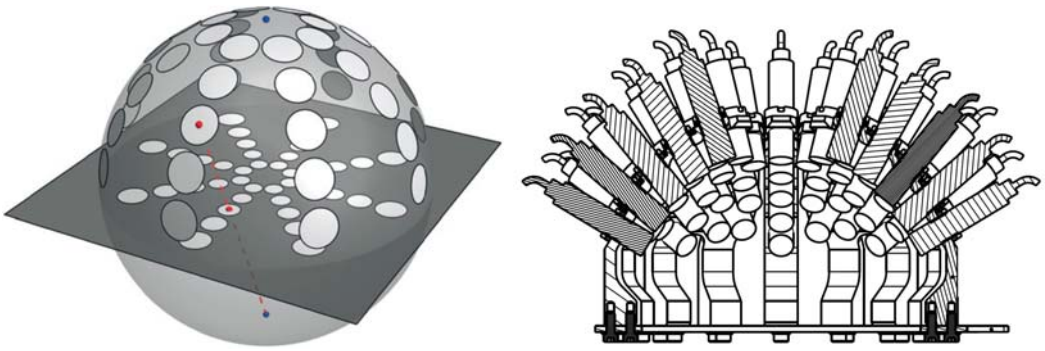

(a) (b)

Figure 2.2: Hemispherical illumination. (a): Lighting pattern of Gruna [4]. (b) Setup of Schöch et al. [5].

Gruna [4] as well as Schöch et al. [5] both utilize several individual light sources, which are located on a hemisphere, cf. Figure 2.2. By activating them individually or in groups, the direction of illumination can be controlled in a targeted manner. However, the illumination direction of the individual elements cannot be altered once they are adjusted. Therefore, we propose a light field display as a universal lighting approach for visual inspection systems.

3 Proposed Method

A light field display is a planar light source in which both the position and the direction of light emission can be controlled independently and simultaneously. Our prototype combines a monitor with an array of lenses mounted in front of it at a distance corresponding to the focal length of the individual lenses, cf. Figure 3.1. Whenever a pixel is activated behind an individual lens, the light field display emits a parallel bundle of rays in a direction determined by the spatial position of the activated pixel behind the individual lens. This generates a 4D light field and enables a customizable illumination from many individual spatial positions and angular directions at once.

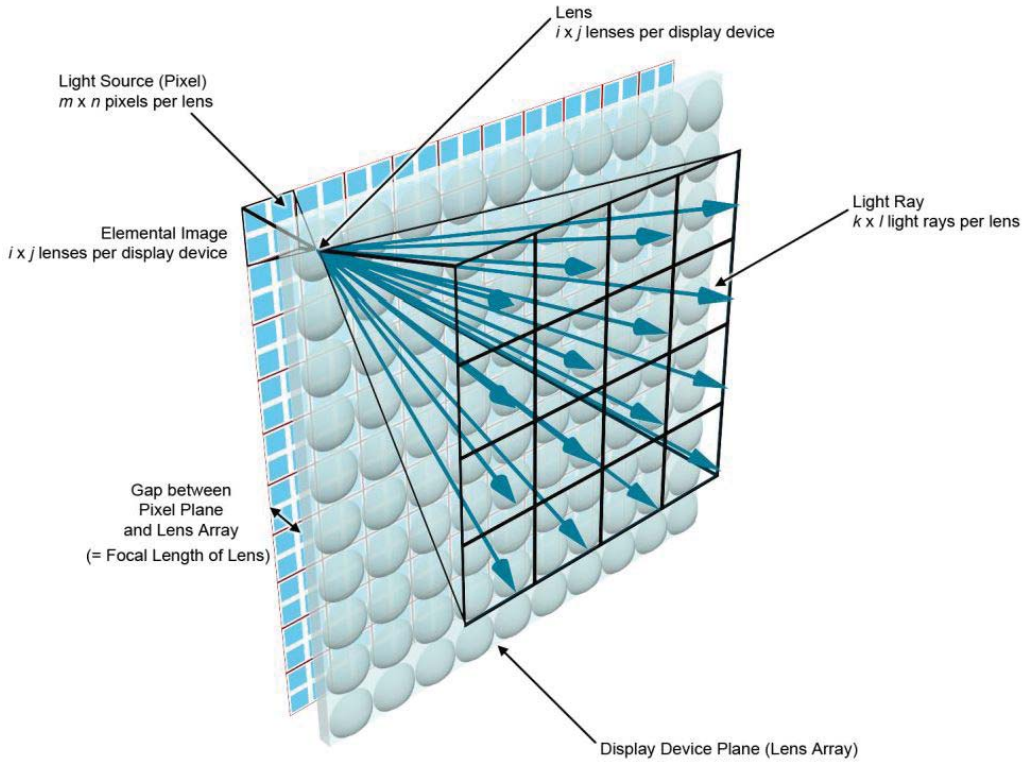

Figure 3.1: Basic setup of a light field display. From [6]. Both the spatial position and the angular direction of the light emission ca be controlled simultaneously.

4 Technical Realization

The light field emitted by a light field display can be adjusted in four dimensions. It allows for two degrees each of spacial and angular freedom. Since the light field display converts between the two-dimensional image displayed on its monitor and the emitted light field purely physically, the challenge in displaying the wanted light field lies with converting the four-dimensional input into a two-dimensional representation which can be displayed by the monitor.

$$L(x, y, \phi, \gamma) \xrightarrow{rendering} I(u, v) \xrightarrow[conversion]{optical} L'(x, y, \phi, \gamma) \tag{4.1}$$

The exact transformation required is determined by a variety of factors such as the pixel density of the screen used, the size and optical properties of each micro-lens and the arrangement of these lenses relative to the screen pixels.

In order to be able to control the light field, it is necessary to know precisely which monitor pixel is responsible for emitting light in a specific direction. The assignment of each monitor pixel to a spatial pixel (individual lens) and a directional pixel (observation angle) is conducted by means of the following calibration routine.

Calibration The goal is to determine the exact position of the central pixel behind each micro lens. Light emitted from these center pixels is collimated by the lens array into a bundle of rays that extends perpendicularly from the monitor.

The position of the center pixels corresponds to the position of the individual lenses in the plane of the lens array. Based on this relationship, the emission angles of the neighboring pixels can be computed.

To achieve this, we place a camera with a telecentric lens in front of the light field display with its optical axis aligned vertically to it. Now the captured light rays origin from these very center pixels.

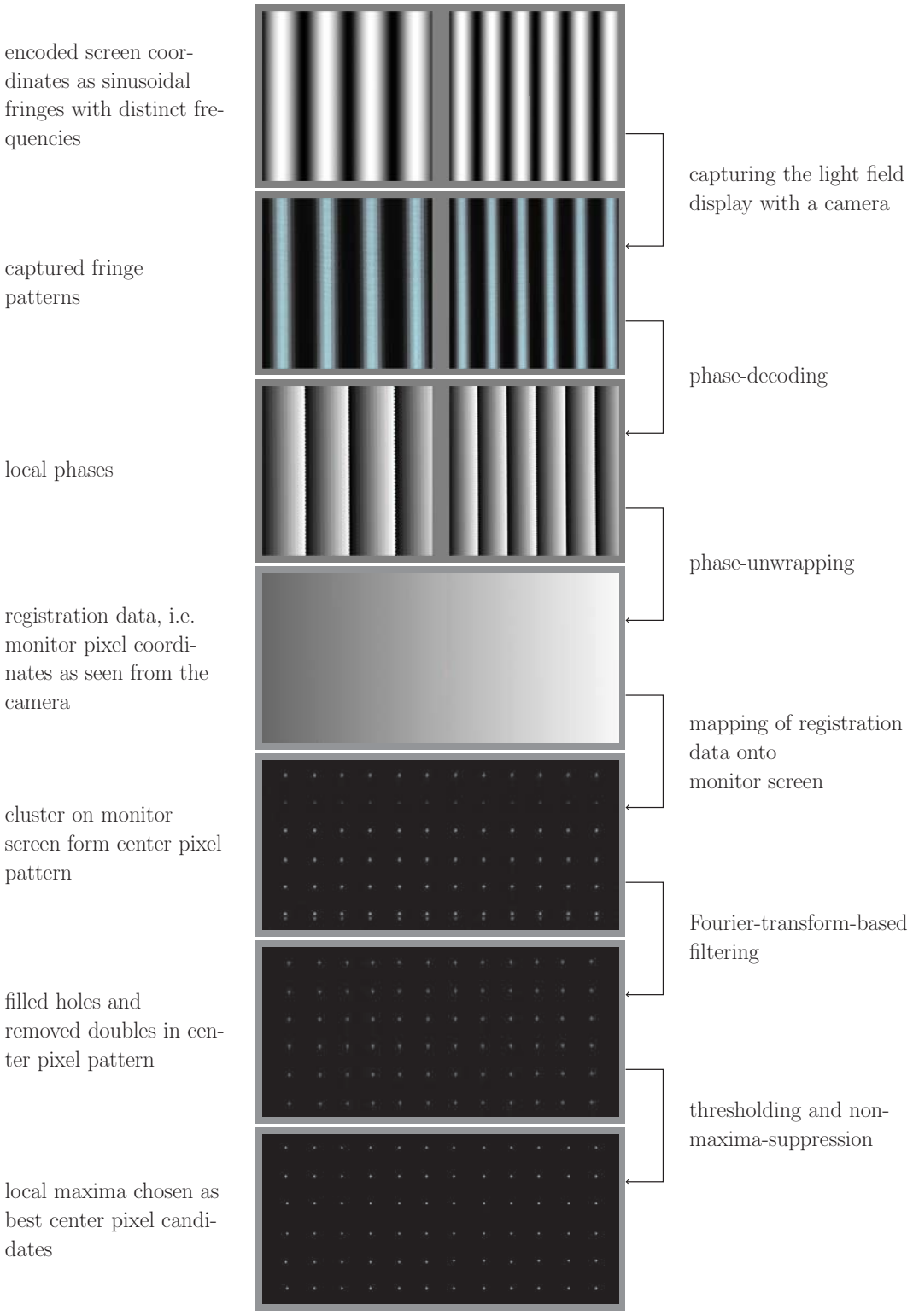

Figure 4.1: Visual representation of the calibration procedure. The goal is to determine the exact position of the center pixels behind each micro-lens.

We determine their exact positions by means of a coded illumination sequence. We deploy temporal phase shifting with two sets of sinusoidal fringes with different wavelength each. Once their phases are decoded locally, their global position is computed by multi frequency temporal phase unwrapping. Here, each camera pixel acts as an individual sensor as opposed to spatial unwrapping approaches, where neighboring pixels are used. Hence, the unwrapping is robust when measuring complex objects with discontinuities and isolated surfaces such as the one of the micro-lens array.

Mapping the number of occurrences of each position results in clusters around the center pixel positions. Their spread (Figure 4.2) origins mainly from the spherical shape of the individual lenses, not focusing in a point but rather in a point spread function. Also, whenever the optical axis of a micro-lens does not intersect with the center of a single pixel, but rather with the intersection of two (four) neighboring ones, the distribution will be spread at least over those two (four) pixels. Since the spatial distance between monitor pixels and micro-lenses are not integer multiples of each other, these two cases will alternate periodically. This effect is known as incommensurability. As a result, the light field display is unable to emit perfectly collimated light. However, the effect is rather small, cf. Figure 5.3.

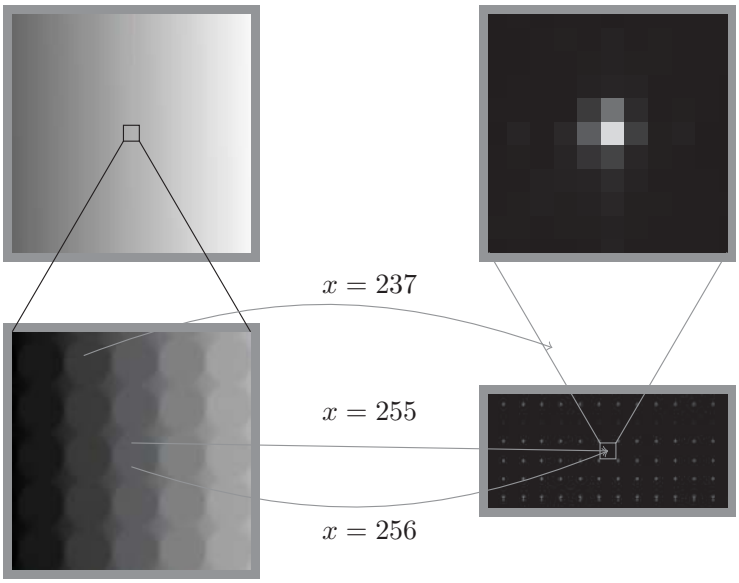

Figure 4.2: Mapping the registration data onto the monitor screen reveals clusters around the center pixel positions.

Error Correction Although the calibration process is very robust, disturbing factors can lead to errors in the decoded positions of center pixels. Most notably, the occlusion of lenses or parts thereof can result in center pixels whose position is not represented by occurrences above the general noise level. The position of these is therefore lost in the process. In order to avoid such false negatives, additional information in form of global regularity in the position of center pixels can be used. This requires the micro-lenses to actually be arranged in a regular grid, which is the normal case for implementations of light field displays. Hence, this regularity results in distinct maxima when transformed to the Fourier space. Any error constitutes a disturbance of the regular pattern, which in turn adds additional frequencies, cf. Figure 4.3. Their amplitudes correlate with the disturbance's fraction within the pattern. Since these errors generally do not occur following a regular pattern, and their occurrence is rather rare, the amplitudes of these frequencies are quite small and can be filtered by thresholding. After inverse Fourier transformation, this yields a map of center pixels with filled holes and removed doubles. Finally, we simply approximate each center pixel by the integer pixel closest to its optimal position.

Rendering The center pixels form the base for rendering 2D-representations of light fields. The spatial dependency of the light field is controlled by addressing all pixels behind one micro-lens, i. e. all pixels which are closest to one distinct center pixel.

The calibration procedure is not limited to determining the center pixels of each lens, but will more generally yield the positions of all pixels emitting light in any direction the camera captures them from. Therefore, by repeating the procedure with the camera turned by the horizontal and vertical angles ϕ and γ relative to the light field display's normal, one can obtain the positions of all pixels emitting light in this direction. As described by Meyer et al. [7], the resulting pattern is the same as that of the center pixels, but translated by a certain pixel offset Δu and Δv.

Alternatively, we can exploit the geometrical dependencies of the light field display. Assuming the pixel size m and the focal length f of the lenses is known and consistent throughout the micro-lens

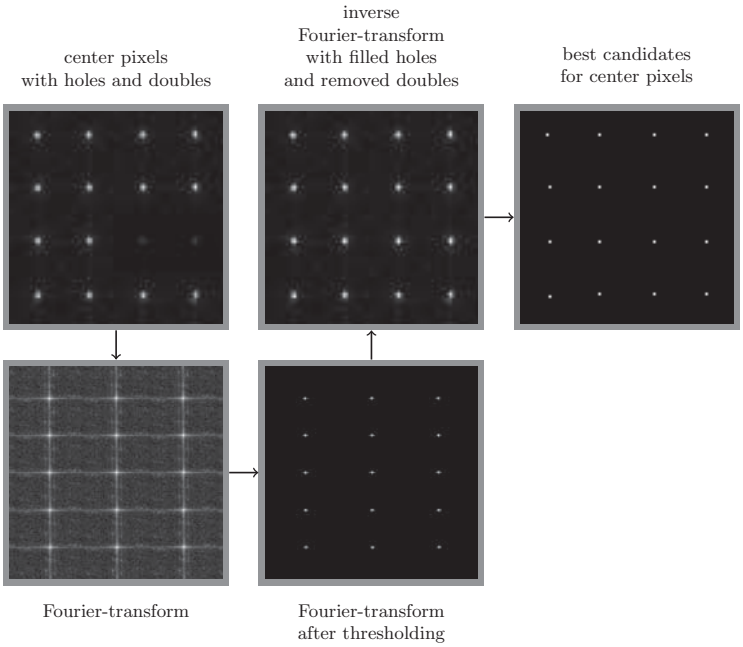

Figure 4.3: Error correction. Irregularities in the grid such as holes and doubles are compensated for using a threshold filter in Fourier domain.

array, determining the angle in which a pixel at a distance Δu resp. Δv relative to the center pixel of each lens will emit light is straight forward:

$$\phi = \arctan\left(\frac{m \cdot \Delta u}{f}\right), \quad \gamma = \arctan\left(\frac{m \cdot \Delta v}{f}\right) \tag{4.2}$$

Using this method, all pixels neighboring the center pixel are utilized to control the angular dependency of the light field.

5 Experiments

To ensure the procedures described above work as expected, we tested them on a light field display constructed from a smartphone featuring a 4K (3840 x 2160 pixels) screen and an array of 100 x 100 micro-lenses with a diameter of 645 µm and a focal length of 3mm each. This corresponds to a total range of possible emission angles of ±6° and an angular resolution of 0.6°.

Figure 5.1 was taken with only the determined center pixels active while the camera remained in the same position from which the

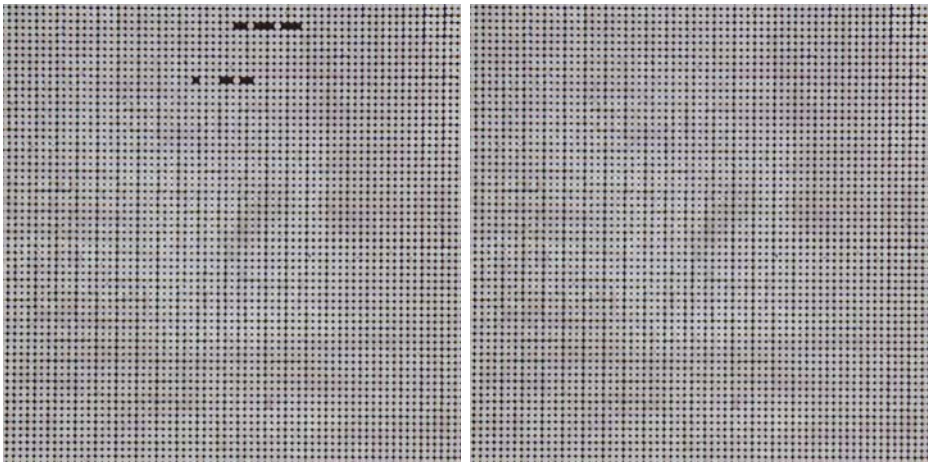

Figure 5.1: Activating only the center pixels determined by the calibration routine before (left) and after (right) error correction.

calibration was conducted. Bright micro-lenses correspond to correctly identified center pixels. After error correction, we are able to correctly address 100% of the center pixels.

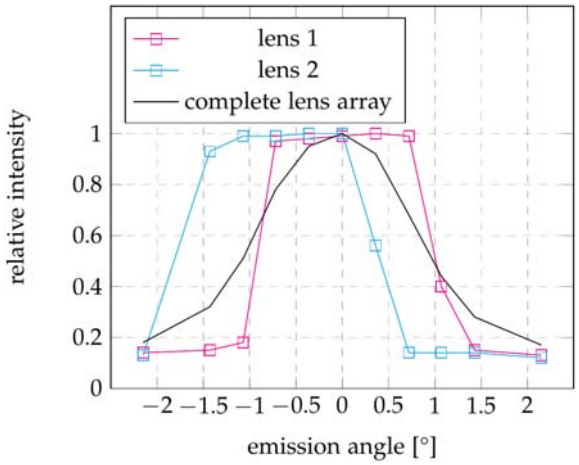

Figure 5.2: With the appropriate rendering (top), different colors are emitted into three distinct directions, each 3° apart. The images taken from the corresponding viewpoints (bottom).

Figure 5.2 shows the angular dependency of the light field display when only the center pixel is activated. The colored graphs depict two extreme cases of single lenses deviating from the targeted emission angle of 0°. They are probably caused by the integer pixel approximation which deviated most from the optimum when the

optical axis of the lenses point at pixel boundaries. The black graph represents the overall angular emission distribution, which is indeed centered at 0°.

The emission angle of ±1° at full width half maximum is caused by minor misalignment of the lens array relative to the smartphone display. Because the actual light emission takes place at an unknown distance beneath the cover glass, the correct focal distance of 3mm is difficult to adjust. For this reason and mostly for the fact that the light is not emitted from a point but a spatially extended area, i. e. the actual pixel, perfectly collimated light beams are impossible to achieve.

Figure 5.3 demonstrates that the light field display's angular selectivity can perfectly be utilized for visual inspection. We projected a spatially uniform light field consisting of three collimated beams into three distinct directions, each 3° apart and encoded them with the base colors red, green and blue. As expected, the light field display appears red, green or blue, depending on the viewing angle. Hence, it can be used to create lighting setups comparable to those shown in Figure 2.1.

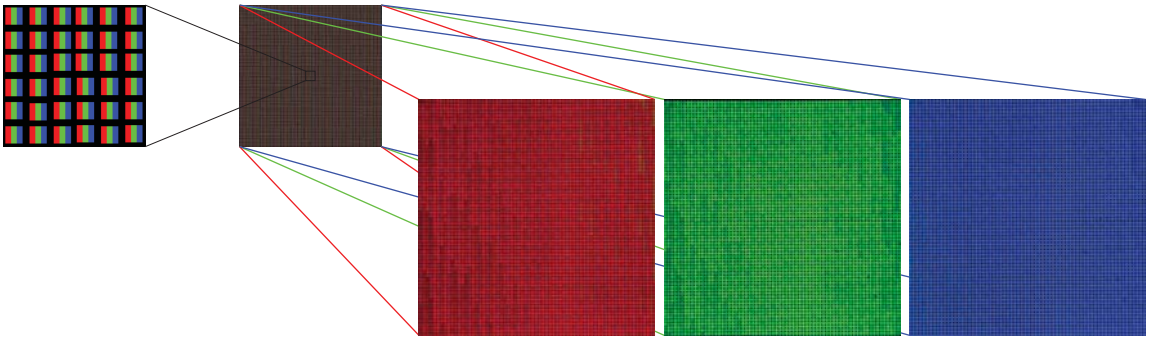

Figure 5.3: With the appropriate rendering (top), different colors are emitted into three distinct directions, each 3° apart. The images taken from the corresponding viewpoints (bottom).

The number of individual addressable angles corresponds to the number of monitor pixels behind each micro-lens. Our prototype is able to emit light into 19 x 19 = 361 different directions. Therefore, much more detailed light fields can be generated. In order to demonstrate the possibilities when controlling both spatial and angular dimensions of the light field, we simulated different perspectives of a

magic cube, cf Figure 5.4. In a second step, we rendered this synthetical light field data into the 2D-representation which is displayed on the smartphone display. The lens array then converts this into a 4D light field, which we captured with a camera from nine different viewpoints. As can be seen, the emitted light field closely resembles the original light field data.

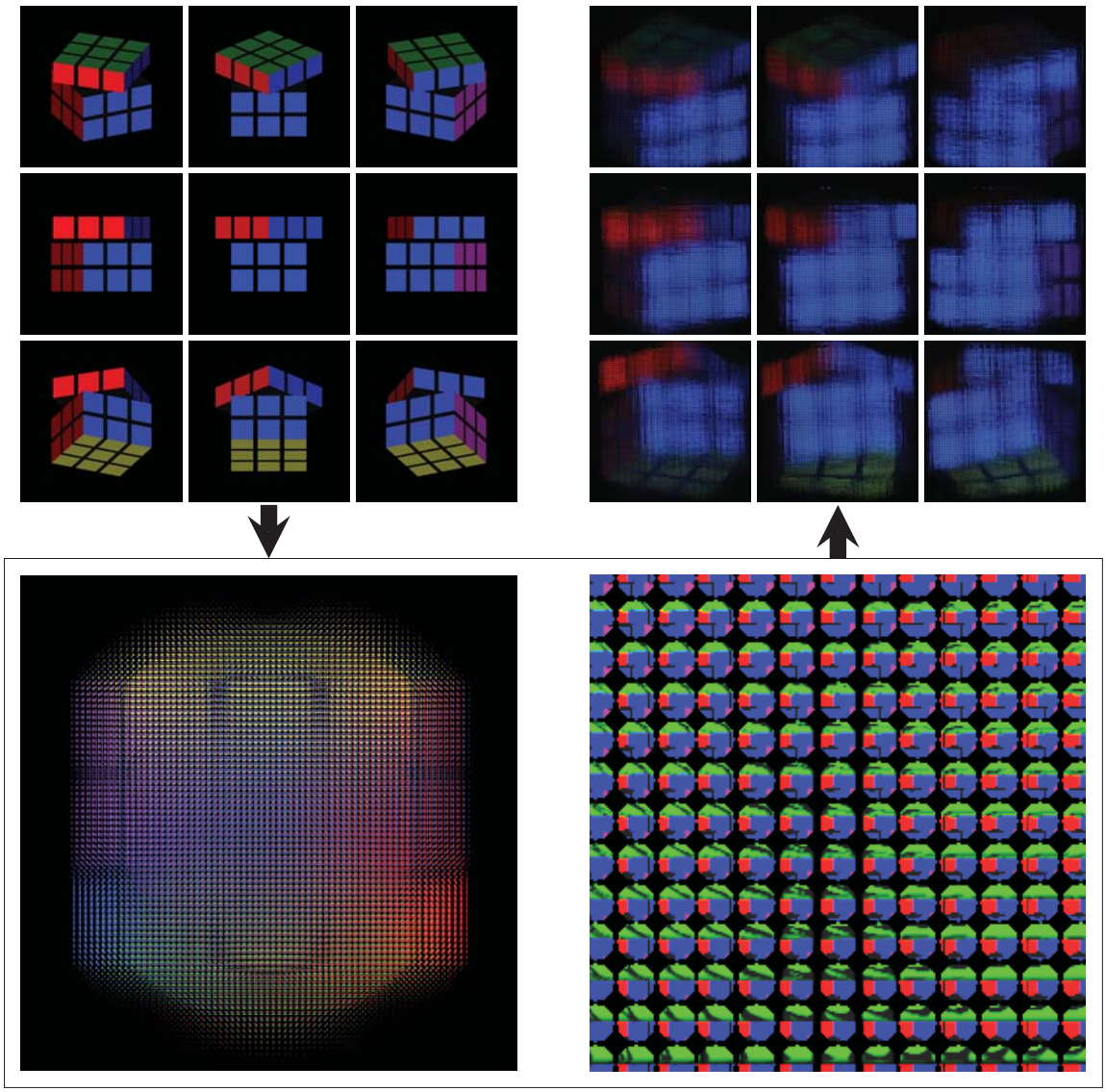

Figure 5.4: Light field rendering and imaging. Synthetic light field data of a magic cube (top left) used to render a 2D-representation optimized for the light field display used (bottom left, detailed bottom right) and the resulting light field emitted from the light field display as seen from different viewing angles (top right). The emitted images closely match the original light field data.

6 Conclusion

Because of the high number of different perspectives used in Figure 5.4, for an observer the magic cube appears as a real 3D-object floating in space. Accordingly, we are able to simulate any light source within the physical constraints of the light field display such as the spectral emission range and the pixel resolution of the monitor.

The latter ultimately limits the spatial and angular resolution of the light field display. Generally, angular dense light fields combined with a broad emission angle and a reasonable spatial resolution of the lens array can only be realized with monitors whose pixels are packed extremely dense. Currently, the limits are 807PPI at 4K resolution (3840 × 2160 pixels) [8] for smartphone displays, which are rather small, and 280PPI at 8K resolution (7680 x 4320 pixels) [9] for larger screens up to 32".

The next step after generating light fields from synthetic data is to use recorded light fields. They can be used to realize an inverse light field illumination for visual inspection. The challenge is not only to precisely capture the light field caused by an object, but also to recode its four-dimensional, spatial-angular data to meet the physical properties of the device emitting the inverse light field.

References

1. Stemmer Imaging AG, "The Imaging & Vision Handbook," www.stemmer-imaging.com, 2020. [Online]. Available: https://www.stemmer-imaging.com/de-de/handbuch-der-bildverarbeitung/
2. Fraunhofer IOSB. (2020, Jun.) Purity-Qualitätsprüfung transparenter Objekte. https://www.iosb.fraunhofer.de/servlet/is/5208/. [Online]. Available: https://www.iosb.fraunhofer.de/servlet/is/5208/
3. J. Beyerer, *Machine Vision : Automated Visual Inspection : Theory, Practice and Applications*, F. Puente León and C. Frese, Eds. Berlin: Springer, [2016]. [Online]. Available: http://d-nb.info/1071728458/04;http://deposit.d-nb.de/cgi-bin/dokserv?id=5282917&prov=M&dok_var=1&dok_ext=htm;http://swbplus.bsz-bw.de/bsz456265708cov.htm

4. R. Gruna, “Beleuchtungsverfahren zur problemspezifischen Bildgewinnung für die automatische Sichtprüfung,” Ph.D. dissertation, Karlsruher Institut für Technologie (KIT), 2013.
5. A. Schöch, P. Perez, and S. Linz-Dittrich, “Automated classification of imperfections and dust un small optical elements,” in *Forum Bildverarbeitung 2018. Hrsg.: T. Längle, P. L. Fernando, M. Heizmann*. KIT Scientific Publishing, Karlsruhe, 2018, pp. 161–172.
6. R. Matsubara, Z. Y. Alpaslan, and H. S. El-Ghoroury, “Light field display simulation for light field quality assessment,” in *Stereoscopic Displays and Applications XXVI*, N. S. Holliman, A. J. Woods, G. E. Favalora, and T. Kawai, Eds., vol. 9391, International Society for Optics and Photonics. SPIE, 2015, pp. 116 – 130. [Online]. Available: https://doi.org/10.1117/12.2083438
7. J. Meyer, “Light Field Methods for the Visual Inspection of Transparent Objects,” Ph.D. dissertation, Karlsruher Institut für Technologie (KIT), 2018.
8. Sony Europe B.V., “Sony Xperia XZ Premium - Technische Daten,” www.sony.de, 2020. [Online]. Available: https://www.dell.com/de-de/work/shop/accessories/apd/210-amfd#techspecs_section
9. Dell Technologies Inc., “Dell UltraSharp 32 PremierColor UltraHD 8K,” www.dell.com, 2020. [Online]. Available: https://www.dell.com/de-de/work/shop/accessories/apd/210-amfd#techspecs_section